

Electronic Supplementary Information for:

## Oxidation-induced activation of chalcogen bonding in redox-active bis(selenomethyl)tetrathiafulvalene derivatives

Maxime Beau,<sup>a</sup> Olivier Jeannin,<sup>a,b</sup> Marc Fourmigué,<sup>\*a</sup> Pascale Auban-Senzier,<sup>b</sup> Frédéric Barrière,<sup>a</sup>  
Ie-Rang Jeon<sup>\*a</sup>

<sup>a</sup>Univ Rennes, CNRS, ISCR (Institut des Sciences Chimiques de Rennes), Campus de Beaulieu, 35000 Rennes, France.

<sup>b</sup>Laboratoire de Physique des Solides UMR 8502 CNRS-Université Paris-Saclay, Bat 510, 91405 Orsay cedex, France

[ie-rang.jeon@univ-rennes1.fr](mailto:ie-rang.jeon@univ-rennes1.fr)

[marc.fourmigue@univ-rennes1.fr](mailto:marc.fourmigue@univ-rennes1.fr)

---

### Table of Contents

<b>Experimental Section</b>	<b>S2</b>
<b>Table S1:</b> Crystallographic table	<b>S4</b>
<b>Figure S1:</b> <sup>1</sup> H NMR of <b>1</b>	<b>S5</b>
<b>Figure S2:</b> <sup>13</sup> C NMR of <b>1</b>	<b>S6</b>
<b>Figure S3:</b> <sup>1</sup> H NMR of <b>2</b>	<b>S7</b>
<b>Figure S4:</b> <sup>13</sup> C NMR of <b>2</b>	<b>S8</b>
<b>Figure S5:</b> Projection view of neutral <b>1</b> along <i>a</i> axis and an ellipsoid plot of <b>1</b>	<b>S9</b>
<b>Figure S6:</b> Structure of neutral <b>2</b>	<b>S10</b>
<b>Figure S6:</b> View of crystal structure of <b>2</b> with 50% thermal ellipsoid	<b>S11</b>
<b>Figure S8:</b> ESP maps of <b>1</b> and <b>2</b>	<b>S12</b>
<b>Figure S9:</b> ESP maps of <b>1</b> <sup>•+</sup> and <b>2</b> <sup>•+</sup>	<b>S12</b>
<b>Figure S10:</b> Structure of <b>(1)Br</b>	<b>S13</b>
<b>Figure S11:</b> View of crystal structure of <b>(1)Br</b> with 50% thermal ellipsoid	<b>S14</b>
<b>Figure S12:</b> Structure of <b>(2)Br</b>	<b>S15</b>
<b>Figure S13:</b> View of crystal structure of <b>(2)Br</b> with 50% thermal ellipsoid	<b>S16</b>
<b>Figure S14:</b> Temperature dependence of the resistivity for a single-crystal of <b>2</b> <sup>•</sup> <b>Br</b> .	<b>S17</b>
<b>Table S2:</b> Literature examples of Se-substituted tetrathiafulvalene radicals showing ChB	<b>S18</b>
<b>Figure S15:</b> Literature examples of Se-substituted tetrathiafulvalene radicals showing ChB	<b>S19</b>
<b>References</b>	<b>S20</b>

## Experimental Section

Reagents were obtained from commercial suppliers and used without further purification. All reactions were carried out under an atmosphere of argon using standard Schlenk techniques. Synthesis of *o*-Me<sub>2</sub>TTF,<sup>1</sup> 4,5-ethylenedithio-1,3-dithiole-2-thione,<sup>2</sup> 4,5-bis(2'-cyanoethylseleno)-1,3-dithiol-2-one<sup>3</sup> were reported previously. Solvents were dried using commercial solvent purification system from Inert Technology. Melting points were measured using a Kofler hot-stage apparatus. NMR spectra were recorded on Bruker Avance 300 MHz spectrometer. Compounds were purified using Teledyne IscoCombiFlash® Rf400. Elemental analyses were performed on a Perkin Elmer 2400 series at the BioCIS.

### 1. Syntheses

**4,5-bis(methylseleno)-6,7-dimethyl-tetrathiafulvalene, *o*-Me<sub>2</sub>TTF(SeMe)<sub>2</sub> (1).** A solution of diisopropylamine (1.21 mL, 8.61 mmol) in dry THF (50 mL) was cooled down to -40 °C. *n*BuLi (2.5M in hexane, 3.6 mL, 8.95 mmol) was added dropwise and the mixture was stirred for 30 min to prepare LDA solution. *ortho*-3,4-dimethyltetrathiafulvalene (800 mg, 3.44 mmol) was dissolved separately in 5 mL of dry and degassed THF and added dropwise to the LDA solution. The mixture turned red and when the temperature rose to -30 °C to result in a yellow precipitate. The mixture was stirred for 2 h and selenium powder (200 mesh, dried under vacuum, 820 mg, 10.39 mmol) was added in one portion. The temperature was allowed to rise to room temperature overnight. The mixture was dark red at this point. Iodomethane (0.54 mL, 8.61 mmol) was added in one portion and stirred for 1 h. THF was then evaporated under reduced pressure, the crude product was dissolved with dichloromethane and washed three times with brine solution. Flash chromatography (24 g SiO<sub>2</sub>, 35 mL / min, solid deposit, gradient 0 to 50 % of dichloromethane in petroleum ether) was performed to obtain 1.05 g of pure product as red powder (2.51 mmol, 73%). The product was recrystallized with EtOAc. m.p. 110 - 112 °C. <sup>1</sup>H NMR (300 MHz, CDCl<sub>3</sub>) δ = 2.33 (s, 6H), 1.94 (s, 6H). <sup>13</sup>C NMR (133 MHz, CDCl<sub>3</sub>) δ = 122.91, 118.85, 112.61, 108.98, 13.85, 9.93. Elemental analysis calcd (%) for C<sub>10</sub>H<sub>12</sub>S<sub>4</sub>Se<sub>2</sub>: C, 28.71; H, 2.89; found: C, 29.08; H, 2.92.

**4,5-ethylenedithio-6,7-bis(2'-cyanoethylseleno)-tetrathiafulvalene.** 4,5-Bis(2'-cyanoethylseleno)-1,3-dithiol-2-one (1.00 g, 2.62 mmol) and 4,5-ethylenedithio-1,3-dithiole-2-thione (0.88 mg, 3.92 mmol) was added to dry toluene (25 mL) under argon atmosphere. The solution was stirred and heated to 80 °C and 25 mL of freshly distilled P(OEt)<sub>3</sub> was added and the solution was stirred for 2 h. Solvents and remaining of P(OEt)<sub>3</sub> were evaporated under rotary vane pump and the compound was isolated by flash chromatography using dichloromethane and petroleum ether as eluent. The product was obtained as red oil (1.19 g, 77%). <sup>1</sup>H NMR(300 MHz, CDCl<sub>3</sub>) δ = 3.30 (s, 2H), 3.09 (d, J=7.7 Hz, 2H), 2.85 (d, J = 6.9 Hz, 2H). Elemental analysis. calcd (%) for C<sub>14</sub>H<sub>12</sub>N<sub>2</sub>S<sub>6</sub>Se<sub>2</sub>: C, 30.10; H, 2.17; N, 5.02; found: C, 30.15; H, 2.61; N, 5.12.

**4,5-bis(methylseleno)-6,7-ethylenedithio-tetrathiafulvalene, EDT-TTF(SeMe)<sub>2</sub> (2).** A solution of 4,5-ethylenedithio-6,7-bis(2'-cyanoethylseleno)-tetrathiafulvalene (100 mg, 0.18 mmol) in anhydrous dimethylformamide (20 mL) was cooled down to 0 °C and then a solution of CsOH· H<sub>2</sub>O (90 mg, 0.54 mmol) in dry MeOH (5 mL) was added dropwise under argon atmosphere. The red/orange solution was stirred for 1.5 h and turned brown. Iodomethane (0.04 mL, 0.63 mmol) was added in one portion at 0 °C and stirring was maintained for 2h. The resulting solution became orange. Solvents were evaporated under reduced pressure and the crude residue was solubilized in dichloromethane, washed with water and dried over MgSO<sub>4</sub>. Solvents were evaporated under reduced pressure and the compound was purified by flash chromatography on 12 g silica gel column. Elution with a gradient 0 → 30% of DCM in petroleum ether gave the compound as a red thick oil (84 mg, 0.17 mmol, 98%). The compound was crystallized by cooling

a hot MeCN solution. m.p. 82 °C.  $^1\text{H}$  NMR (300 MHz,  $\text{CDCl}_3$ )  $\delta$  = 3.29 (s, 4H), 2.33 (s, 6H).  $^{13}\text{C}$  NMR (300 MHz,  $\text{CDCl}_3$ )  $\delta$  = 118.64, 118.11, 113.99, 107.46, 30.25, 9.89. Elemental analysis. calcd (%) for  $\text{C}_{10}\text{H}_{12}\text{S}_4\text{Se}_2$ : C, 25.00; H, 2.10; found: C, 25.52; H, 2.33.

## 2. Electrocrystallizations

They were performed in two-compartment cells with Pt electrodes (length 1 cm, diameter 1 mm) under aerobic condition. Crystals of **1•Br** and **2•Br** were obtained from the electrocrystallization of **1** (10 mg) and **2** (10 mg) in  $\text{CH}_3\text{CN}$  (10 mL taken from the solvent purification system) at room temperature in the presence of  $\text{PPh}_4\text{Br}$  and  $\text{NEt}_4\text{Br}$ , respectively, as the electrolyte. A constant current of 0.1 and  $1\mu\text{A}$ , respectively, was applied during 7 days. Black crystals were harvested from the electrode once the current source is removed.

## 3. X-ray crystallography

Single crystals of **1**, **2**, (**1**)**Br** and (**2**)**Br** that are suitable for X-ray analysis were coated with Paratone-N oil and mounted on a MicroMounts<sup>TM</sup> rod. X-ray diffraction measurements were performed on a Bruker APEX II diffractometer operating with a Mo  $\text{K}\alpha$  ( $\lambda = 0.71073 \text{ \AA}$ ) X-ray tube with a graphite monochromator. Structures were solved by dual-space algorithm using SHELXT<sup>4</sup> and then refined with full-matrix least-square methods based on  $F^2$  (SHELXL-2014)<sup>5</sup> with the aid of the WINGX program.<sup>6</sup> All non-hydrogen atoms were refined with anisotropic atomic displacement parameters. H atoms were finally included in their calculated positions. The refinement of **2** has been done on the basis of HKLF 5 file, generated with TWINABS, constructed from all observations involving the first domain and merged according to point-group  $2/m$ . The single reflections that also occur in composites have been omitted. The two components (65/35 ratio) are related through a rotation angle of  $179.35^\circ$  around the  $-1\ 0\ -0.01$  vector in the direct space. Crystallography data (in cif format) have been deposited with deposition numbers CCDC 2190022-2190025. Crystallographic data and the details of data collection are listed in Table S1.

## 4. Resistivity measurements

The resistivity measurements were performed along the long axis of the needle-shaped crystal of (**2**)**Br**. Four gold wires were directly glued with silver paste on the crystal. Four probes resistivity measurements were performed with a DC current of  $0.3\mu\text{A}$  using a Keithley 2400 Source Meter (Data shown in Figure S14). The same temperature dependence was obtained with a four probes AC method, applying a current of  $1\mu\text{A}$  and low-frequency ( $<100 \text{ Hz}$ ) with lock-in amplifier detection. Low temperature was provided by a homemade cryostat equipped with a 4 K pulse-tube.

## 5. Theoretical calculations

Calculations of  $\beta_{\text{HOMO-HOMO}}$  interaction energies were based upon the effective one-electron Hamiltonian of the extended Hückel method,<sup>7</sup> as implemented in the Caesar 1.0 chain of programs.<sup>8</sup> The off-diagonal matrix elements of the Hamiltonian were calculated according to the modified Wolfsberg-Helmholz formula.<sup>9</sup> All valence electrons were explicitly taken into account in the calculations and the basis set consisted of double-z Slater-type orbitals for all atoms except H (single-z).

Electrostatic potential calculations were carried out on the optimized geometry of the molecules (with density functional theory using the Gaussian 16, Revision C.01 software, the B3LYP functional and the 6-31+G\*\* basis set for all atoms). GaussView 5.0.9 was used to generate the figures. The calculated ESP maps are presented in 0.001 e/bohr<sup>3</sup> isosurface (1 bohr = 1 atomic unit (a.u.) = 0.529177249 Å).

**Table S1** | Crystallographic data of **1**, **2**, **(1)Br** and **(2)Br**.

	<b>1</b>	<b>2</b>	<b>(1)Br</b>	<b>(2)Br</b>
CCDC code	2190022	2190025	2190024	2190023
Empirical formula	C <sub>10</sub> H <sub>12</sub> S <sub>4</sub> Se <sub>2</sub>	C <sub>10</sub> H <sub>10</sub> S <sub>6</sub> Se <sub>2</sub>	C <sub>10</sub> H <sub>12</sub> S <sub>4</sub> Se <sub>2</sub> Br	C <sub>10</sub> H <sub>10</sub> S <sub>6</sub> Se <sub>2</sub> Br
Formula weight, g mol <sup>-1</sup>	418.36	480.46	498.27	560.36
Crystal system	Monoclinic	Monoclinic	Monoclinic	Monoclinic
Space group	P2 <sub>1</sub> /c	P2 <sub>1</sub> /c	P2 <sub>1</sub> /n	P2 <sub>1</sub> /c
Wavelength, Å	0.71073	0.71073	0.71073	0.71073
Temperature, K	296	150	298	296
<i>a</i> , Å	16.179(9)	15.7509(18)	7.0207(9)	5.8409(4)
<i>b</i> , Å	8.230(5)	13.2011(13)	11.2279(13)	17.6599(12)
<i>c</i> , Å	11.342(7)	15.8501(16)	19.282(3)	16.2327(9)
$\alpha$ , °	90	90	90	90
$\beta$ , °	96.59(3)	105.818(3)	92.628(6)	93.323(2)
$\gamma$ , °	90	90	90	90
<i>V</i> , Å <sup>3</sup>	1500.2(15)	3170.9(6)	1518.4(3)	1671.58(19)
<i>Z</i>	4	8	4	4
$\mu$ , mm <sup>-1</sup>	5.458	5.43	8.03	7.55
<i>Reflections coll./unique</i>	10468/2161	17029/4212	2358/1567	40223/2962
<i>R(int)</i>	0.0564	0.079	0.1079	0.057
<sup>a</sup> <i>R</i> <sub>1</sub> ( <i>I</i> > 2σ( <i>I</i> ))	0.0635	0.059	0.055	0.085
<sup>b</sup> w <i>R</i> <sub>2</sub> (all)	0.1535	0.1344	0.144	0.036
GoF	1.041	1.008	0.98	1.05

<sup>a</sup>*R*<sub>1</sub> =  $\Sigma||F_0| - |F_c|| / \Sigma|F_0|$ , and <sup>b</sup>w*R*<sub>2</sub> =  $[\Sigma w(F_0^2 - F_c^2)^2 / \Sigma w(F_0^2)^2]^{1/2}$

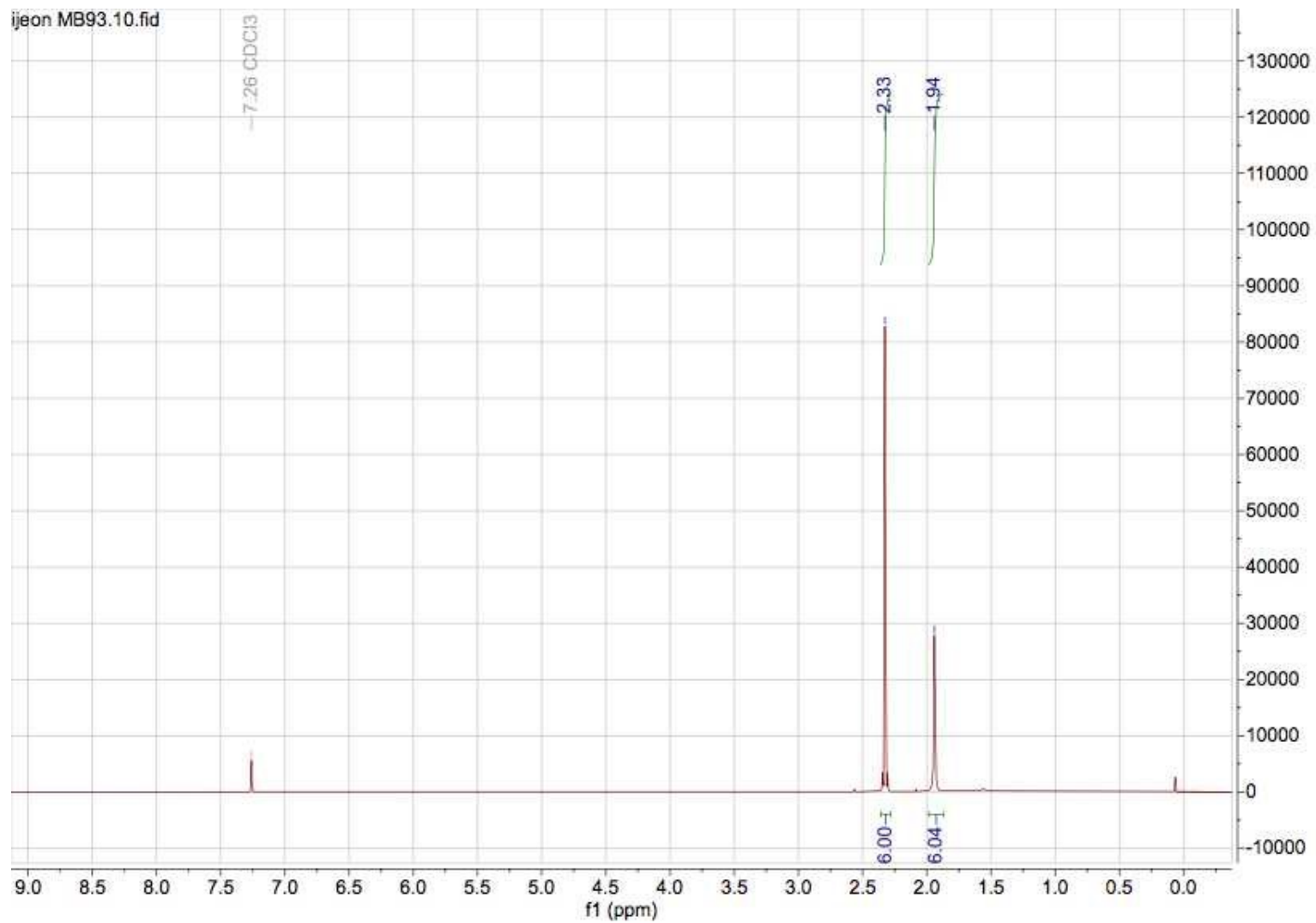


Figure S1 | <sup>1</sup>H NMR of **1** in CDCl<sub>3</sub>.

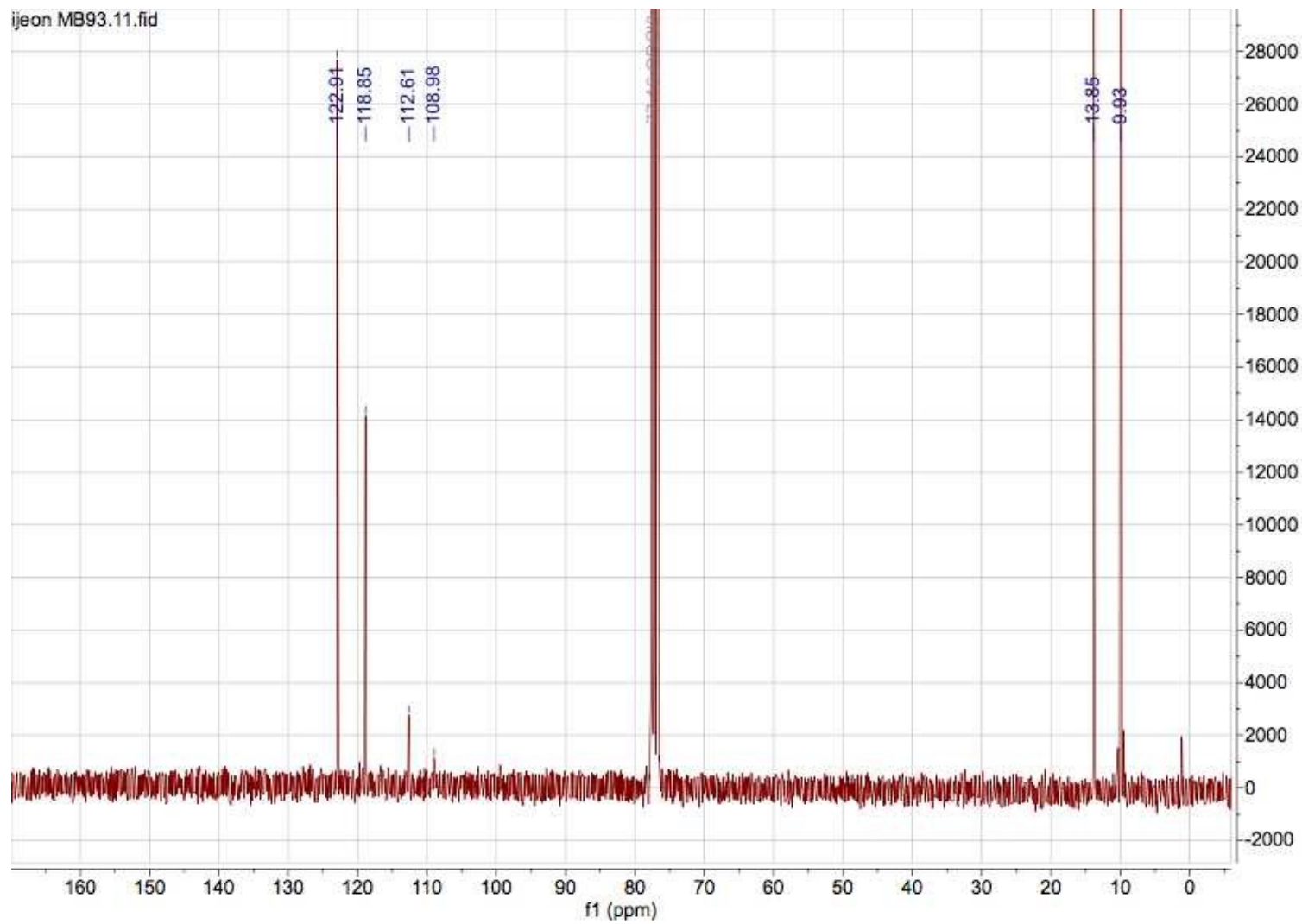


Figure S2|  $^{13}\text{C}$  NMR of **1** in  $\text{CDCl}_3$ .

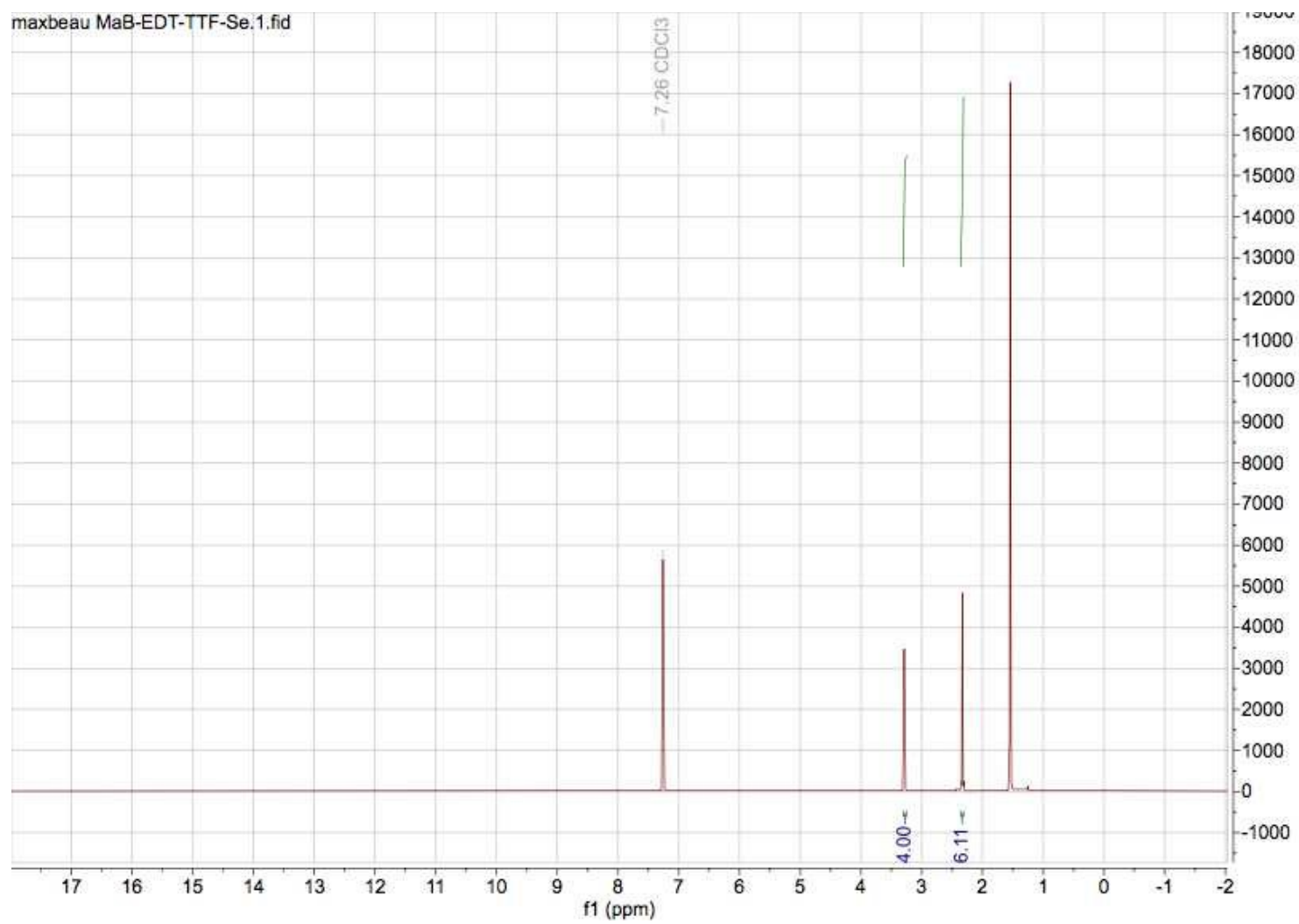


Figure S3 | <sup>1</sup>H NMR of **2** in CDCl<sub>3</sub>.

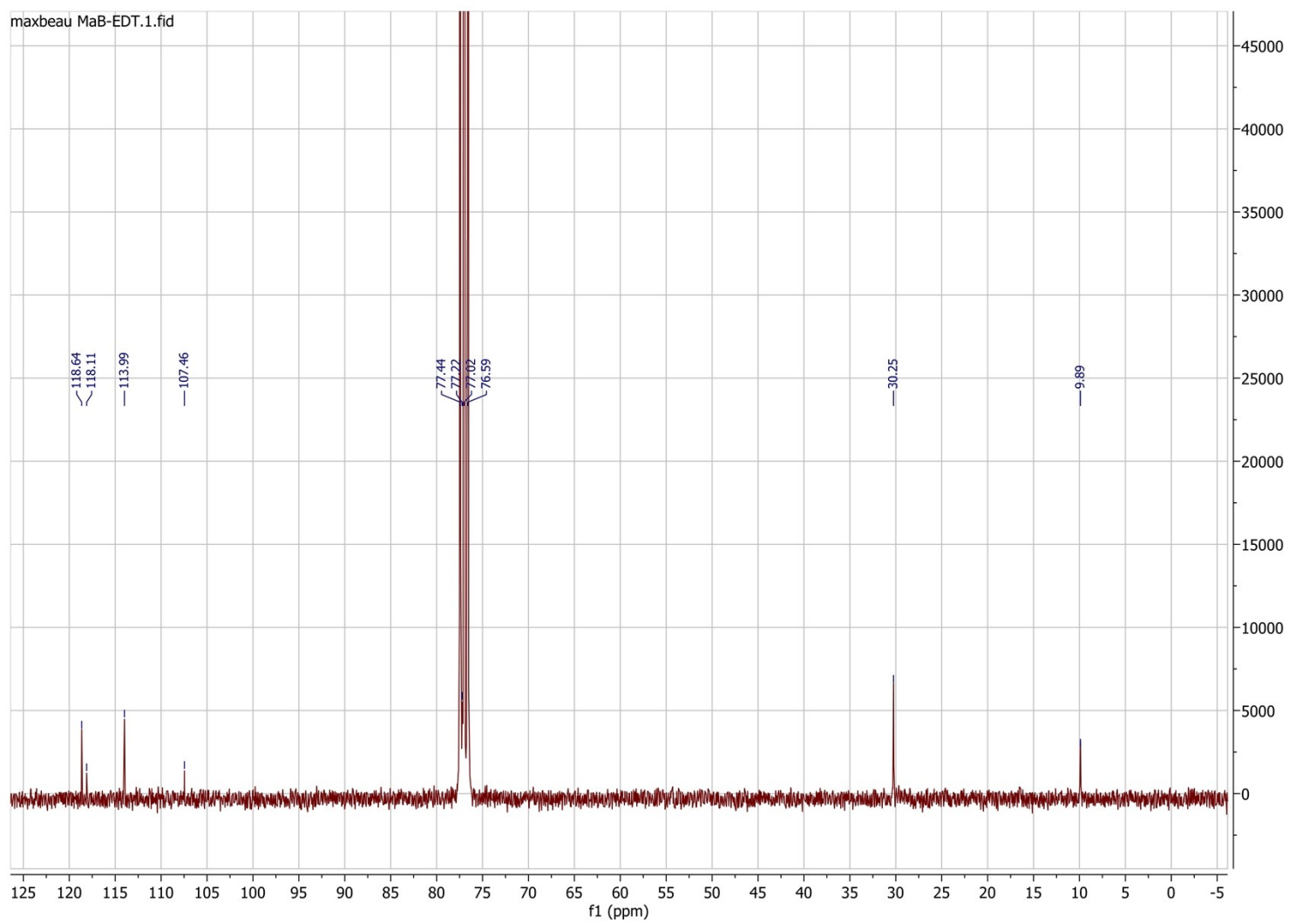
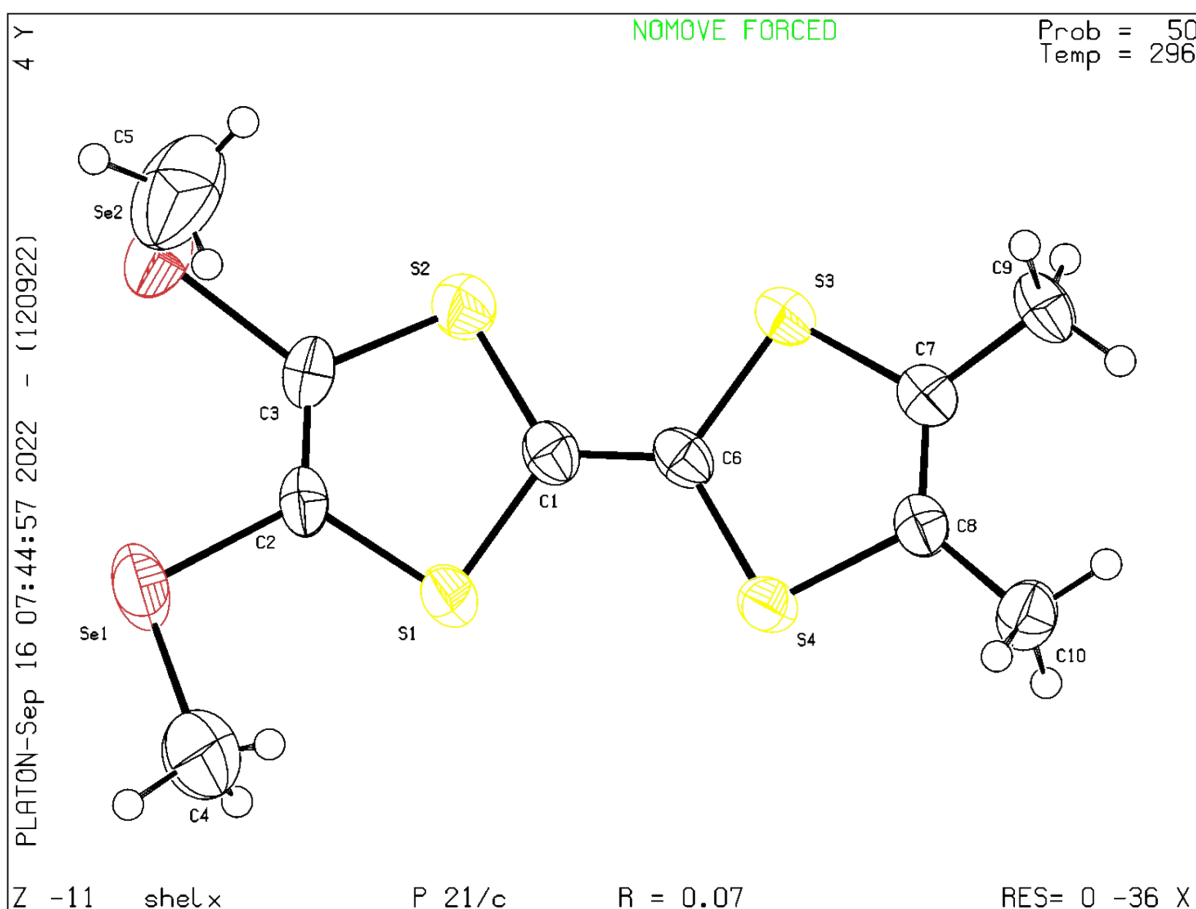
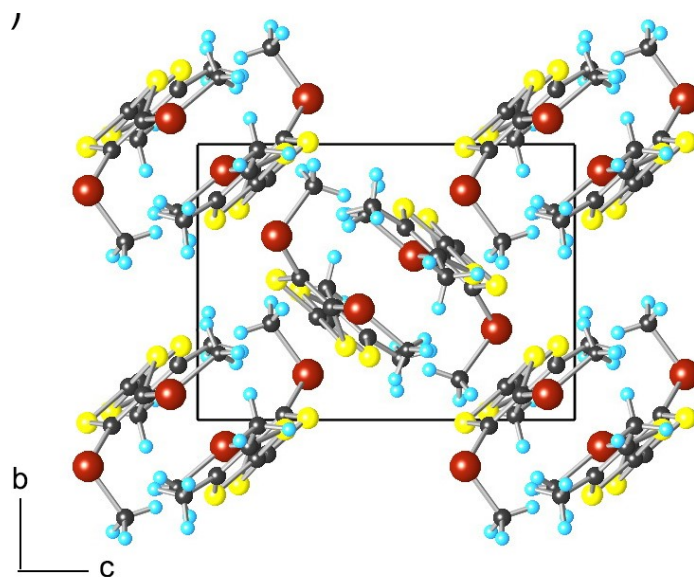
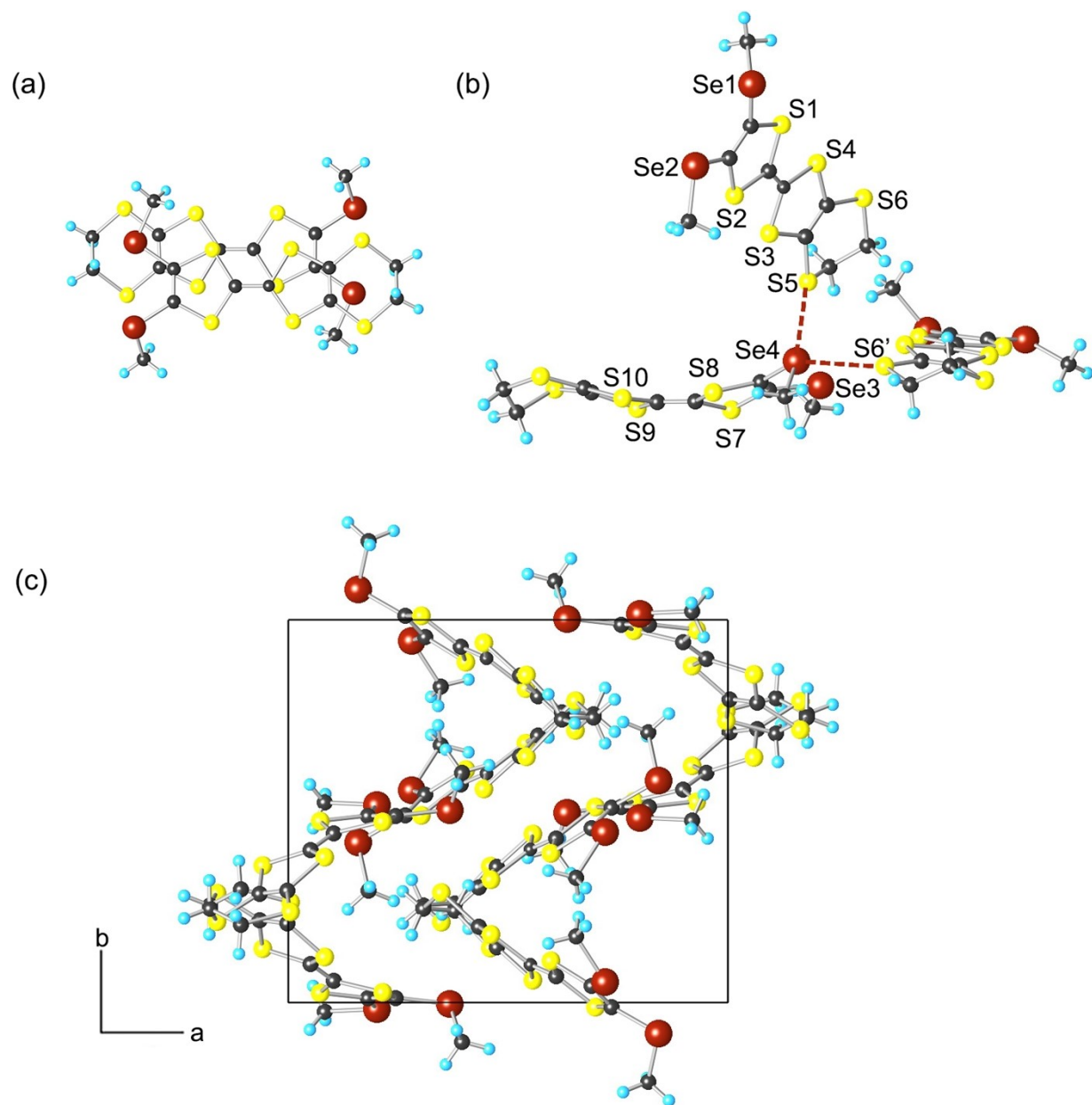


Figure S4 |  $^{13}\text{C}$  NMR of **2** in  $\text{CDCl}_3$ .



**Figure S5** | Projection view of neutral **1** along *a* axis (upper) and an ellipsoid plot of **1** (lower).



**Figure S6** Structure of neutral **2** with (a) overlap pattern within a dimer; (b) short contacts; (c) projection view along *c* axis.

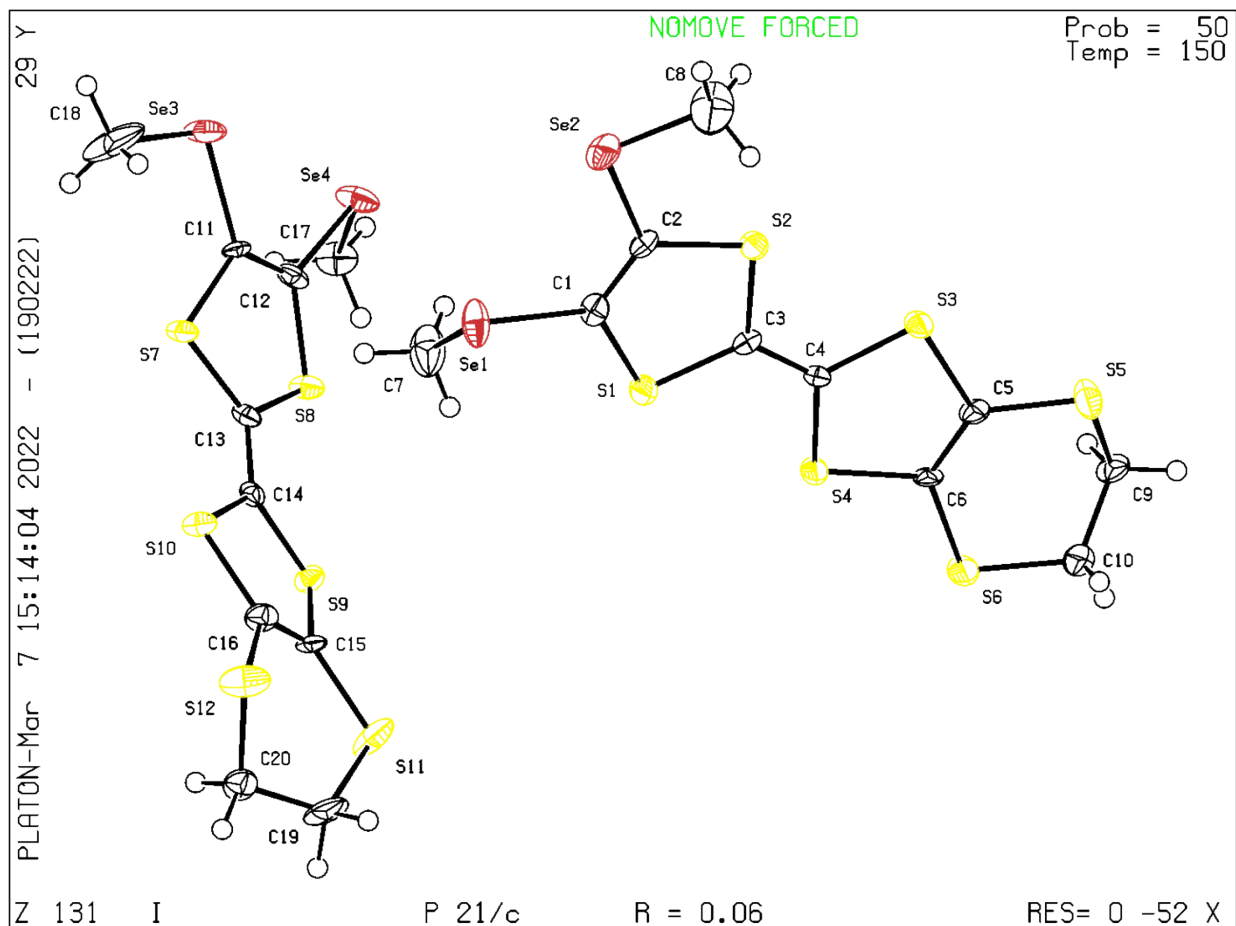


**Figure S7** | View of crystal structure of **2** with 50% thermal ellipsoid

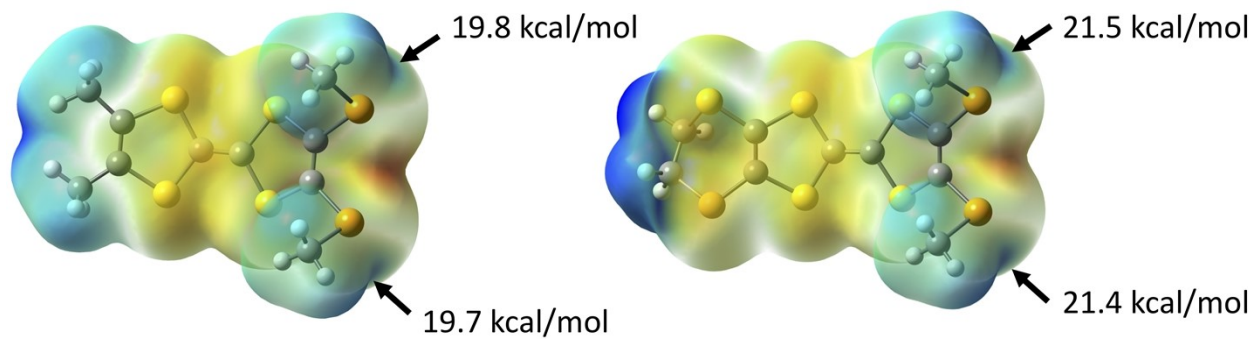


**Figure S8** | ESP maps of **1** (left) and **2** (right) at 0.001 e/bohr<sup>3</sup> isosurface with  $V_S$  values on Se atoms in kcal/mol. Potential scales from -28.2 (red) to +28.2 (blue) kcal/mol.

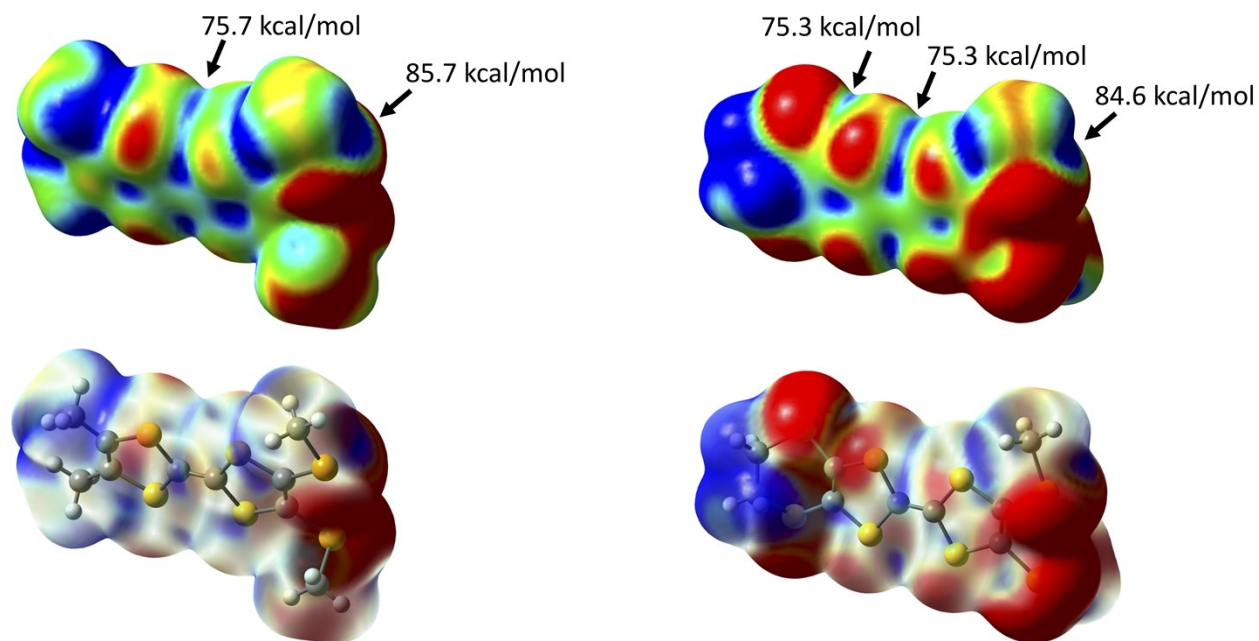


**Figure S9** | ESP maps of **1<sup>+•</sup>** (left) and **2<sup>+•</sup>** (right) at 0.001 e/bohr<sup>3</sup> isosurface with  $V_S$  values in kcal/mol. Potential scales from +62.8 (red) to +76.6 (blue) kcal/mol, to better visualize electropositive areas.

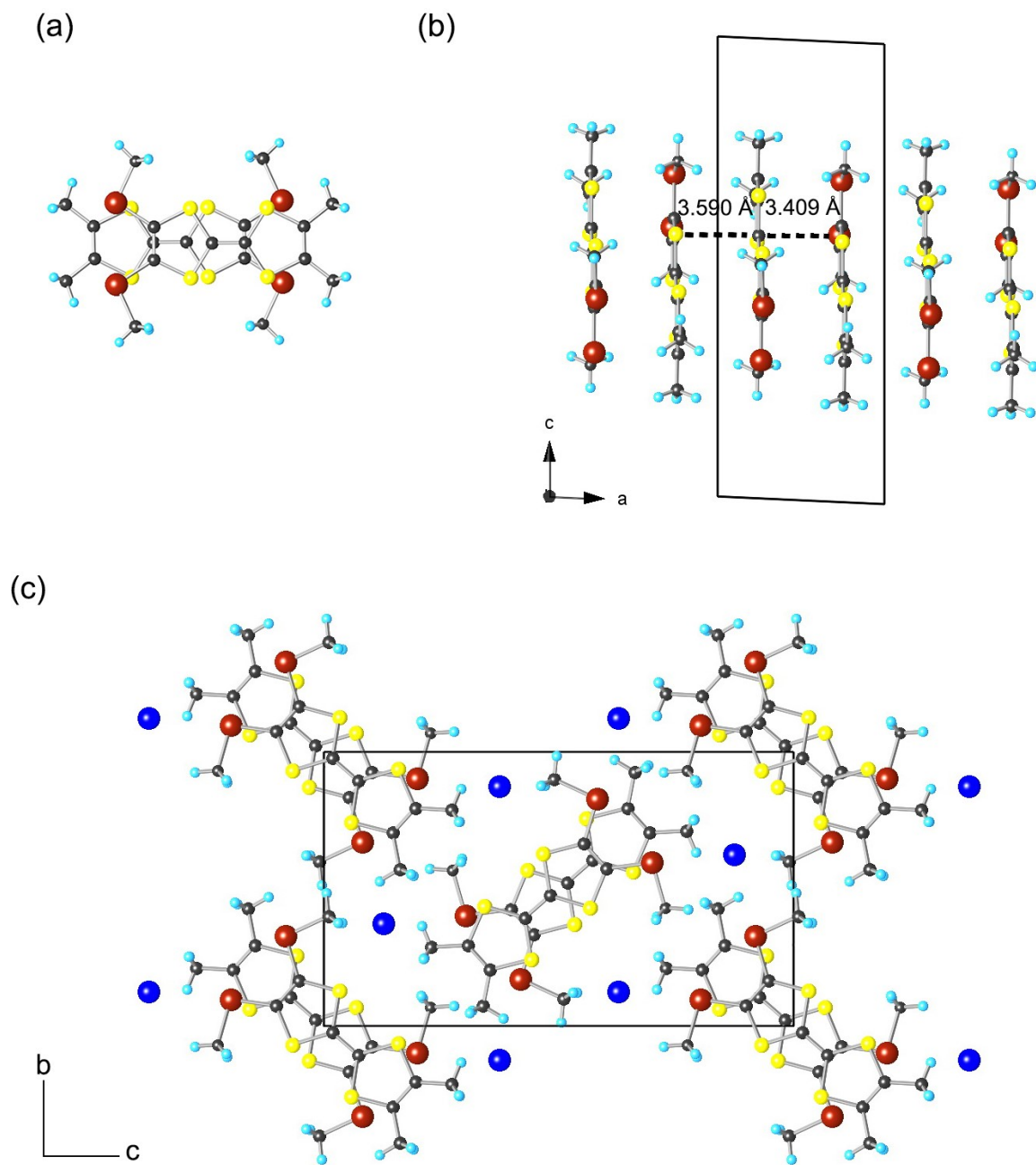


**Figure S10** | Structure of **(1)Br** with (a) overlap pattern within a dimer; (b) projection view along *b* of one chain of  $1^{+}$  radical cations; (c) projection view along *a* axis.

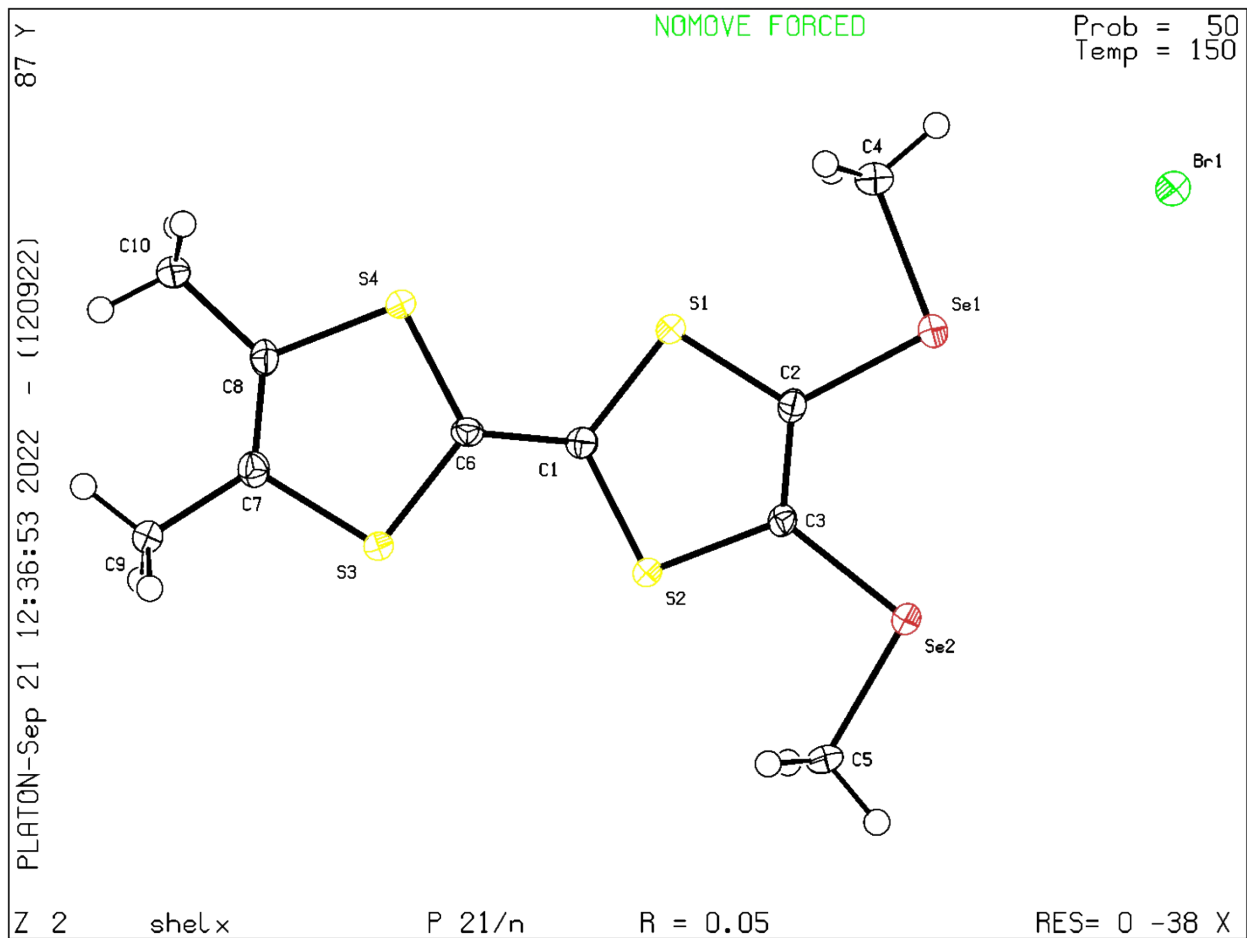


**Figure S11** | View of crystal structure of **(1)Br** with 50% thermal ellipsoid

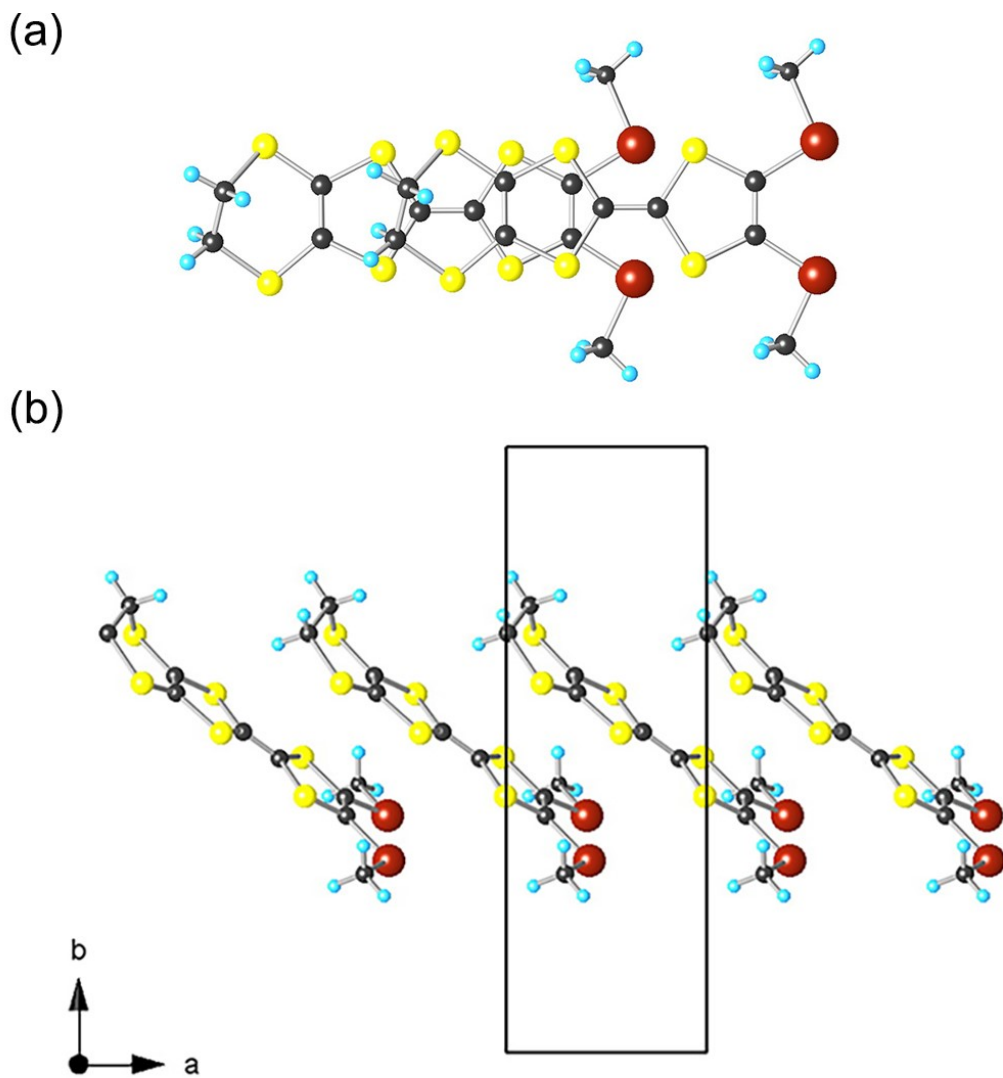


**Figure S12** Structure of **(2)Br** with (a) overlap pattern within a dimer; (b) projection view along *c* of one chain of  $2^{+\bullet}$  radical cations.

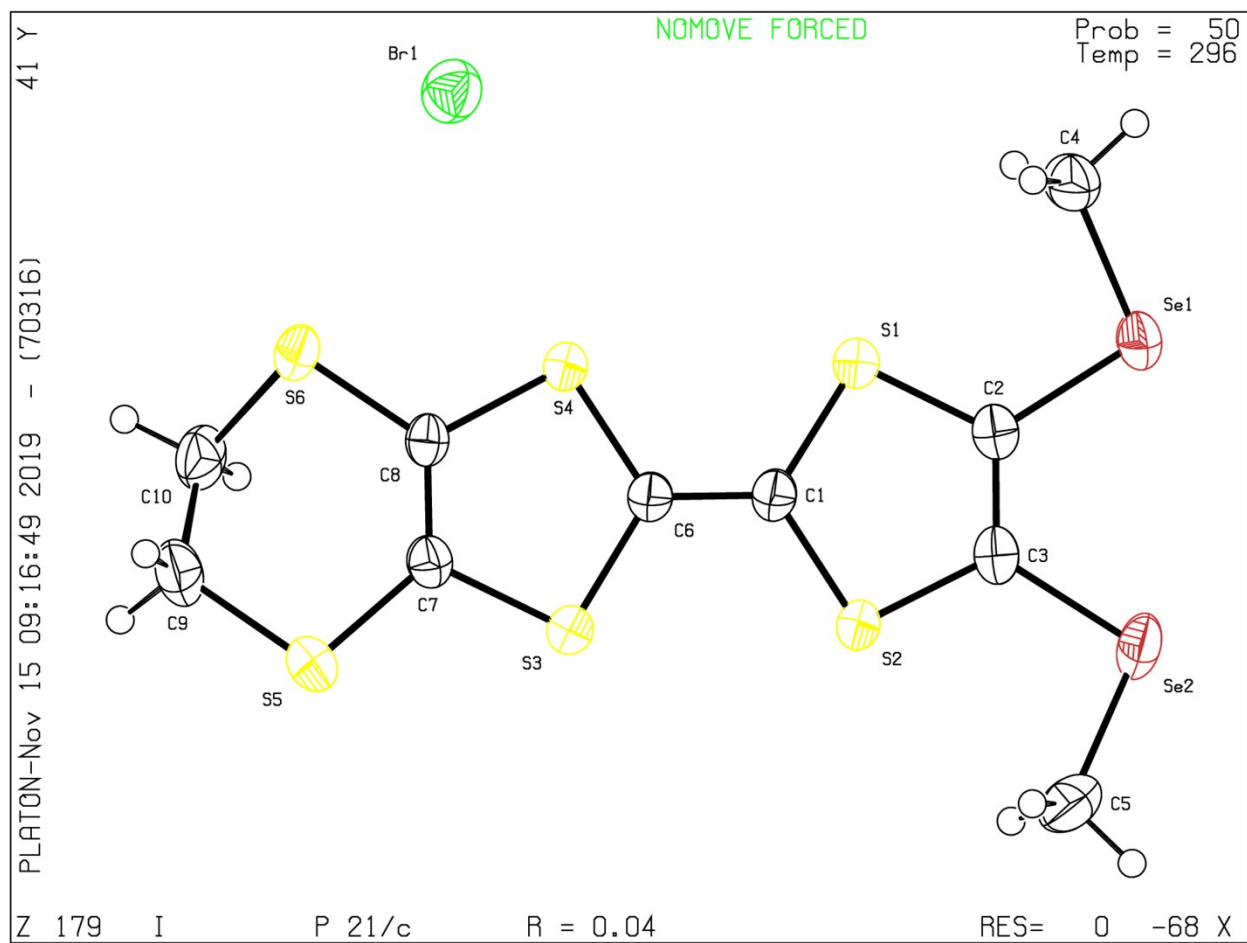
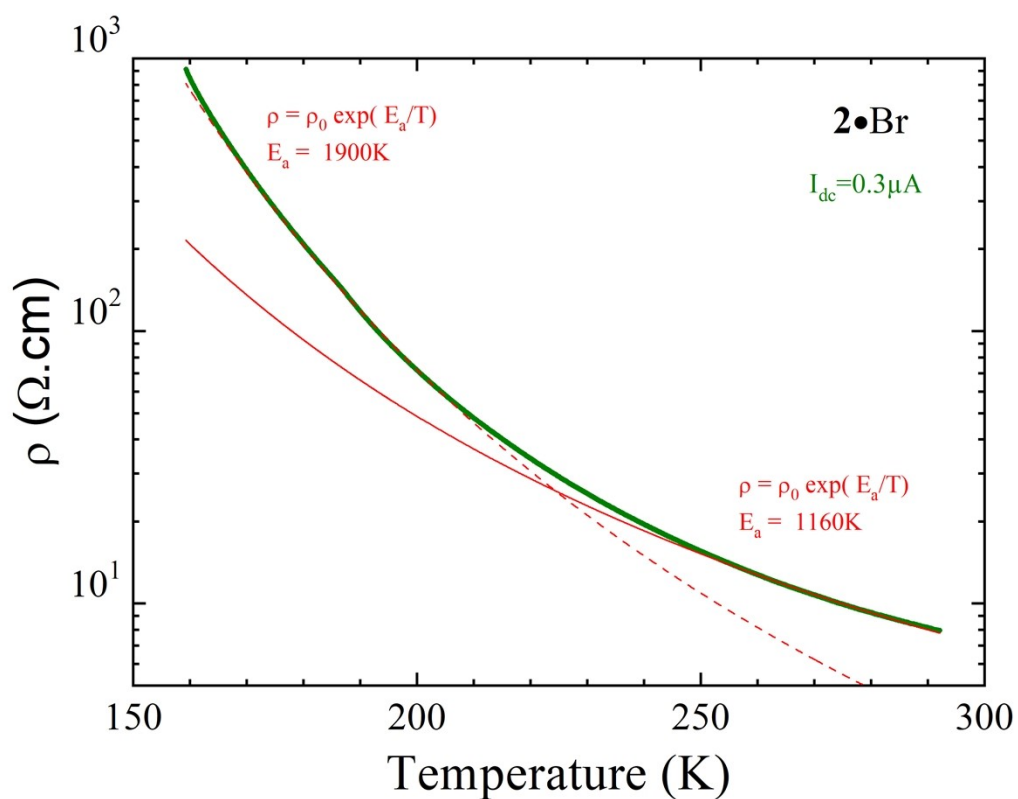
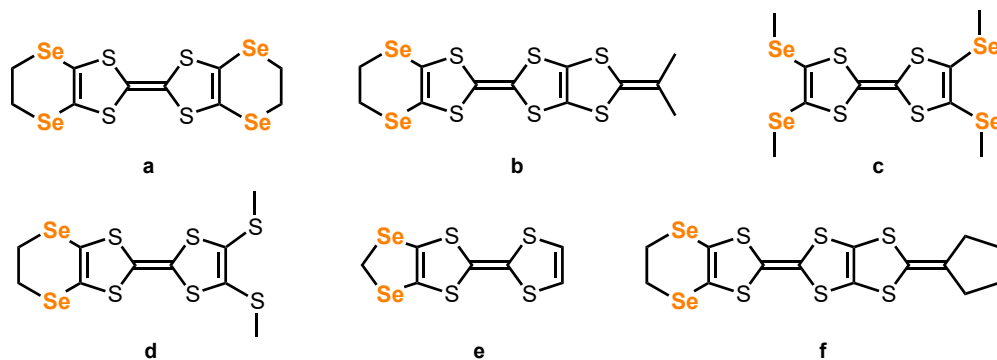


Figure S13| View of crystal structure of (2)Br with 50% thermal ellipsoid



**Figure S14** | Temperature dependence of the resistivity for a single-crystal of **(2)Br**. The red lines are fit to the data with an activation law of the type  $\rho = \rho_0 \exp(E_a/T)$ , the continuous line corresponds to the fit in the high temperature range (250-300K) and the dashed line in the low temperature range (160-200K).

**Table S2** | Literature examples of Se-substituted tetrathiafulvalene radicals showing chalcogen bonding interactions with anions.



CCDC codes	Compound	Chalcogen bond (Å)	Reduction ratio	$\angle\text{C-Se}\cdots\text{X}$ (°)
AKAMOO <sup>10</sup>	<b>a</b> <sub>4</sub> [Fe(CN) <sub>6</sub> ]	Se6 $\cdots$ N1 = 3.157	0.92	149
		Se4 $\cdots$ N1 = 3.169	0.92	135
HODZEH <sup>11</sup>	<b>b</b> <sub>2</sub> [Ag(CN) <sub>2</sub> ]	Se1 $\cdots$ N1 = 3.003	0.87	169
		Se4 $\cdots$ N1 = 3.386	0.89	148
HODZIL <sup>12</sup>	<b>b</b> <sub>2</sub> [Au(CN) <sub>2</sub> ]	Se1 $\cdots$ N1 = 2.995	0.86	169
		Se4 $\cdots$ N1 = 3.382	0.89	158
KERNEA <sup>12</sup>	<b>c</b> [I <sub>3</sub> ]	Se1 $\cdots$ I3 = 3.852	0.99	170
		Se4 $\cdots$ I2 = 3.756	0.96	173
SIVJUD <sup>13</sup>	<b>d</b> [FeBr <sub>4</sub> ]	Se1 $\cdots$ Br2 = 3.642	0.97	155
		Se2 $\cdots$ Br1 = 3.586	0.95	174
WEPWET <sup>14</sup>	<b>e</b> <sub>2</sub> [Au(CN) <sub>2</sub> ]	Se2 $\cdots$ N1 = 3.188	0.92	165
YEBZAI <sup>15</sup>	<b>b</b> [AuCN <sub>4</sub> ]	Se1 $\cdots$ N1 = 3.250	0.94	156
YEBZEM <sup>16</sup>	<b>b</b> [ReO <sub>4</sub> ]	Se1 $\cdots$ O2 = 2.998	0.87	172
		Se2 $\cdots$ O1 = 3.108	0.90	161
YEBZIQ <sup>16</sup>	<b>b</b> [I <sub>2</sub> ]I	Se2 $\cdots$ I5 = 3.636	0.93	161
		Se1 $\cdots$ I1 = 3.601	0.92	154
YEBZOW <sup>16</sup>	<b>f</b> [I <sub>3</sub> ]	Se1 $\cdots$ I2 = 3.606	0.92	164

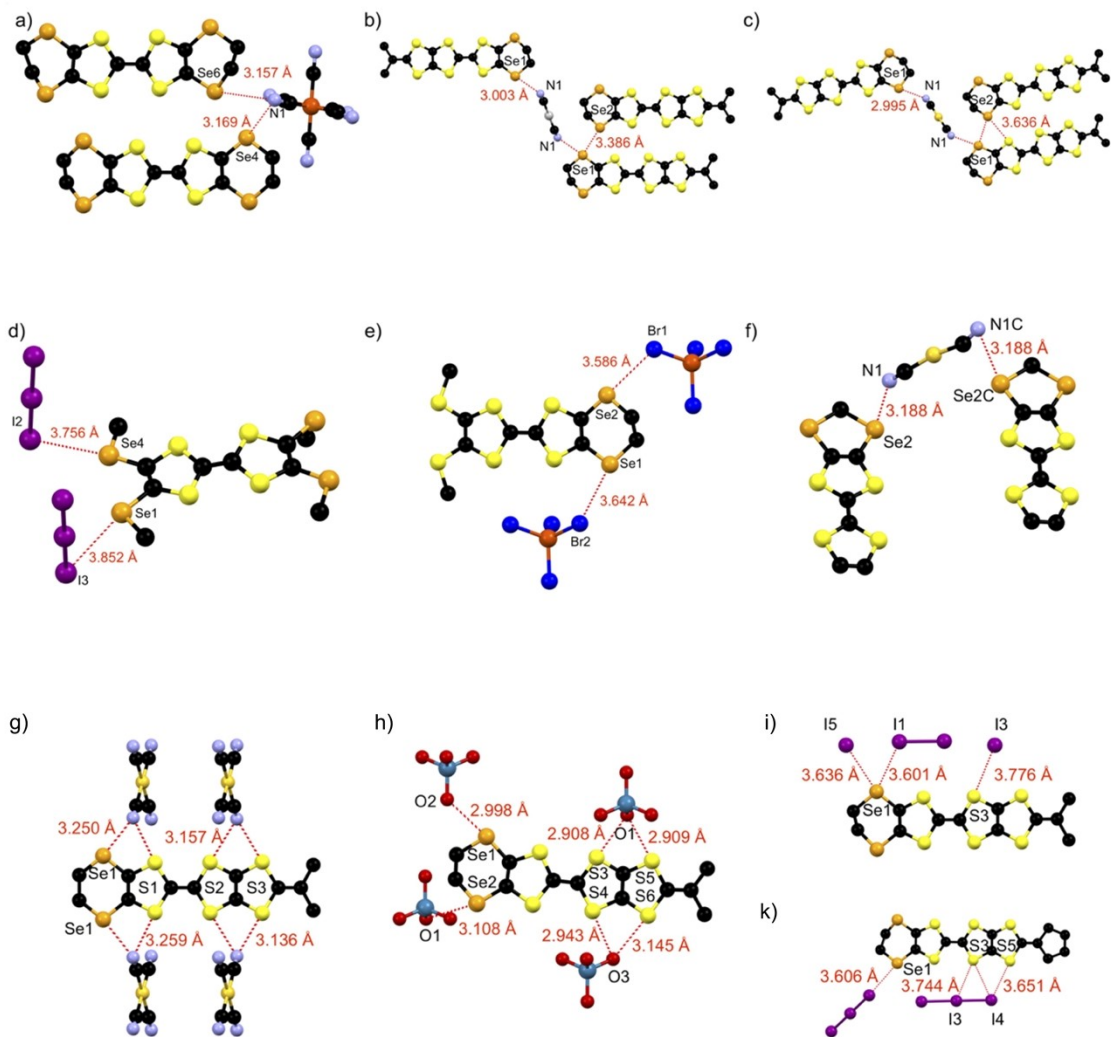


**Figure S15** Literature examples of Se-substituted tetrathiafulvalene radicals showing chalcogen bonding interactions with anions; (a) AKAMOO, (b) HODZEH, (c) HODZIL, (d) KERNEA, (e) SIVJUD, (f) WEPWET, (g) WEPWET, (h) YEBZAI, (i) YEBZEM, (j) YEBZIQ, (k) YEBZOW.

## References

---

- [1] K. Lerstrup, I. Johannsen, M. Jørgensen, *Synthetic Metals* **1988**, 27, 9–13.
- [2] K. B. Simonsen, N. Svenstrup, J. Lau, O. Simonsen, P. Mørk, G. J. Kristensen, J. Becher, *Synthesis* **1996**, 407–418.
- [3] L. Binet, J. M. Fabre, C. Montginoul, K. B. Simonsen, J. Becher, *J. Chem. Soc., Perkin Trans.* **1996**, 783–788.
- [4] G. M. Sheldrick, *Acta Cryst.* 2015, **A71**, 3–8
- [5] G. M. Sheldrick, *Acta Cryst.* 2015, **C71**, 3–8.
- [6] L. J. Farrugia, *J. Appl. Cryst.*, 2012, **45**, 849–854.
- [7] M.-H. Whangbo and R. Hoffmann, *J. Am. Chem. Soc.* **1978**, 100, 6093.
- [8] J. Ren, W. Liang and M.-H Whangbo, *Crystal and Electronic Structure Analysis Using CAESAR*, PrimeColor Software Inc., Cary (NC) USA, 1998
- [9] J. Ammeter, H.-B. Bürgi, J. Thibeault and R. Hoffmann, *J. Am. Chem. Soc.*, 1978, **100**, 3686.
- [10] M. Clemente-Leon, E. Coronado, J. R. Galan-Mascaros, C. Gimenez-Saiz, C. J. Gomez-Garcia, J. M. Fabre, G. A. Mousdis, G. C. Papavassiliou, *J. Solid State Chem.* **2002**, 168, 616.
- [11] K. Furuta, S. Kohno, T. Shirahata, Y. Misaki, *Eur. J. Inorg. Chem.* **2014**, 2014, 3982–3988.
- [12] P. Wang, T. Inabe, C. Nakano, Y. Maruyama, H. Inokuchi, N. Iwasawa, G. Saito, *Bull. Chem. Soc. Jpn.* **1989**, 62, 2252–2257.
- [13] M. Enomoto, A. Miyazaki, T. Enoki, *Bull. Chem. Soc. Jpn.* **2001**, 74, 459–470.
- [14] H. Mori, I. Hirabayashi, S. Tanaka, T. Mori, Y. Maruyama, H. Inokuchi, *Solid State Commun.* **1993**, 88, 411–415.
- [15] K. Furuta, S. Kohno, T. Shirahata, K. Yamasaki, S. Hino, Y. Misaki, *Crystals*, **2012**, 2, 393.